Photonic integrated circuit extended cavity passively mode-locked dual absorber symmetric ring laser

Mu-Chieh Lo[1,2], Dominik Auth[3], Christoph Weber[3], Patrick Fiala[3], Pascal Sauer[3], Guillermo Carpintero[1], and Stefan Breuer[3,*]

[1] Universidad Carlos III de Madrid, Av de la Universidad, 30. 28911 Leganés, Madrid, Spain
[2] University College London, London WC1E 7JE, UK
[3] Institute of Applied Physics, Technische Universität Darmstadt, 64289 Darmstadt, Germany
[*] Corresponding author: stefan.breuer@physik.tu-darmstadt.de

Compiled May 25, 2019

A photonic integrated circuit extended cavity passively mode-locked semiconductor ring laser with two saturable absorbers in a symmetric ring geometry fabricated using an InP generic integration technology platform is presented for the first time. The laser emits 1.4 ps short optical pulses with a time-bandwidth-product of 0.96 (Gaussian shaped pulses) at a fundamental repetition rate of 23.3 GHz. The laser exhibits a beat-note line width of 80 kHz, corresponding to a pulse-to-pulse timing jitter of 31.7 fs. The emission is centered at 1570 nm and maximum spectral bandwidth amounts to 10.2 nm (-3 dB) and 19.7 nm (-20 dB).

OCIS codes: (140.4050) Mode-locked lasers; (140.5960) Semiconductor lasers; (250.5300) Photonic integrated circuits.

http://dx.doi.org/10.1364/ao.XX.XXXXXX

Monolithic passively mode-locked semiconductor lasers are promising compact sources for generating coherent optical frequency combs and ultra-short optical pulse trains for metrology, spectroscopy and millimeter wave/terahertz applications [1]. They reconcile technical simplicity in chip-scale monolithic integration and constant current operation, thus obviating external optical pumping [2]. Compared to their Fabry–Pérot counterparts [3–5], mode-locked semiconductor ring lasers (SRLs) feature the intrinsic mirror symmetry with respect to the central saturable absorber and therefore allow for colliding pulse (CP) mode-locking (ML) [6–10]. By doubling the pulse-narrowing effect, CP ML is expected to decrease the pulse width (PW) and improve the pulse train stability [11, 12]. In early works, a monolithic passively mode-locked GaAs/AlGaAs quantum well based SRL emitting at 860 nm with a 1 mm radius and a single absorber yielded oscillations at 80 MHz to 110 MHz with an inter-mode beat line width (IB LW) of 50 kHz [13], a monolithic passively mode-locked GaAs/AlGaAs quantum well based SRL emitting at 874 nm with a 0.15 mm radius and a single 50 μm long absorber yielded 1.3 ps short optical pulses at an inter-mode beat frequency (IBF) of 86 GHz with a minimum time-bandwidth-product (TBP) of 0.42 [6]. At telecom wavelengths, a monolithic passively mode-locked InP quantum dot SRL emitting at 1505 nm with a length of 18 mm and a single 0.3 mm absorber yielded 55 ps short optical pulses at 5 GHz with an IB LW of 300 kHz (-20 dB), indicating an integrated or root-mean-square (RMS) timing jitter (TJ_{rms}) of 25 ps (integrated from 10 kHz to 80 MHz) [14]. A monolithic passively mode-locked bulk InGaAsP SRL emitting at 1530 nm with a length of 5.291 mm, incorporating two 30 μm or 60 μm long absorbers, generated 4 ps short optical pulses at an IBF of 15 GHz with IB LWs ranging from 2.5 MHz to 5.5 MHz (-20 dB), indicating a TJ_{rms} of 7.1 ps (integrated from 20 kHz to 80 MHz) and a minimum TBP of 0.42 [12]. A monolithic actively mode-locked GaAs/AlGaAs quantum well based SRL emitting at 1543 nm with 3 mm radius and two 0.5 mm long absorbers yielded 27 ps short optical pulses at 9 GHz with a minimum TBP of 0.46 [15]. A passively mode-locked InP quantum well photonic integrated circuit (PIC) SRL emitting at 1583 nm with 33 mm length and a single 50 μm long absorber fabricated using an InP generic integration technology platform generated 9.8 ps short optical pulses, an IBF of 2.5 GHz with an IB LW of 6.13 kHz (-3 dB) at IBF signal-to-noise ratios (SNRs) of >50 dB and optical spectral widths exceeding 3 nm [9]. A PIC InP generic integration technology platform based passively mode-locked quantum well SRL emitting at 1544 nm with 4 mm length and a single 30 μm long absorber yielded estimated 5.6 ps short optical pulses (Gaussian fit to Gaussian shaped pulse) and 0.9 ps ($sech^2$-fit to pulse signature) at an IBF of 20 GHz, an IB LW of 800 kHz (-3 dB) and an IBF SNR of 41 dB [16]. A passively mode-locked InP quantum well SRL with a symmetric ring CP ML geometry on a PIC with 3 mm length and a single 40 μm long absorber emitting at 1565 nm generated 1.9 ps short optical pulses at an IBF of 12 GHz with an IB LW of 390 kHz (-10 dB), an IBF SNR >50 dB and spectral widths exceeding 40 nm (-20 dB) [10]. A monolithic passively mode-locked SRL built on an all-active GaAs/AlGaAs double quantum well platform, emitting at an unknown wavelength, with a length of 3.1 mm and either a single or dual absorbers with 50 μm lengths yielded estimated 9 ps short optical pulses at an IBF of 25 GHz. A symmetric dual-absorber geometry was reported where an increase in ML regime and reduced PWs were expected by pulses colliding only in the absorbers [11]. This dual-absorber SRL could be mode-locked, yet with fewer modes resulting in broader PWs. Additionally, both output waveguides and optical couplers were electrically pumped, thus potentially adversely affecting the generated PW and pulse train stability [11, 12, 17].

In this letter, we report the realization and experimental investigation of a SRL with extended cavity symmetric ring CP ML geometry employing two absorber sections and fabricated using an InP active-passive generic integration technology platform. The PIC laser emits optical pulses as short as 1.4 ps, generates spectral widths exceeding 10 nm (-3 dB) and 19.7 nm (-20 dB) at an IBF of 23.3 GHz with a minimum IB LW of 80 kHz (-3 dB), a clear improvement in PW over the state-of-the-art SRL fabricated by an InP generic integration technology platform.

The cavity design is point symmetric and schematically depicted in Fig. 1(a). It comprises four 300 μm long semiconductor optical amplifiers (SOAs), two 30 μm long saturable absorbers (SAs) and four electro-optic phase modulators (EOPMs). Both SOA and SA sections use the same active layer stack, based on InGaAsP/InP quantum well gain media. The passive straight and curved waveguides form the circulating extended cavity resonance path. The passive waveguides are deeply etched, of 1.5 µm width, minimum bending radii of 100 µm and propagation losses are of the order of 1 dB/cm. Two 2x2 multimode interference (MMI) couplers provide the optical output from the cavity in both, the clockwise (CW) and counter-clockwise (CCW), propagation directions through the output waveguides 1-4 at the edge-cleaved emission facet at the right-hand side. The ring cavity length amounts to ≈3.5 mm, corresponding to an IBF of 23 GHz (refractive index of 3.7). The entire PIC laser design occupies an area of (2.1 x 0.75) mm^2. The laser was fabricated within a multi-project wafer run through the Jeppix foundry coordinator at SMART Photonics with a predefined layer stack [18]. To simplify the operation of the device and avoid breaking the symmetry, the contact pads of the pair of SAs are shorted on the chip. The four SOAs are electrically connected by metal routing. Therefore, the four gain sections are forward-biased with a combined gain current I_{SOA} through one DC probe. Similarly, the two SAs are reverse-biased at the same voltage level V_{SA} by a second DC probe. The EOPMs are left unbiased. A 200 μm long SOA (Boost) is located prior to waveguide Out 3 and can be forward biased by I_{BOOST} to amplify the chip output power when necessary. To minimize parasitic back-reflections, the four output waveguides, corresponding to CW and CCW propagation directions of each 2x2 MMI, are tilted upwards by 7 ° as shown in Fig. 1(a). The cleaved facet is anti-reflection coated reducing the power reflection coefficient to <10^{-4}. Signals Out 1 and Out 3 (with booster) correspond to the CCW propagating pulse train, while Out 2 and Out 4 allow access to the CW direction. In the experiment, the light emitted from optical outputs at the facet are coupled into a lensed fiber as shown in Fig. 1(b). Analysis of the static and spectral laser emission is performed by an optical power meter and an optical spectrum analyzer (OSA) (spectral resolution 10 pm). A nonlinear intensity auto-correlator (AC) characterizes the generated optical PWs. An extended C-band erbium-doped fiber amplifier (EDFA) and a polarization controller increases the output power level and ensures the required polarization state. The IBFs and IB LWs in the pulsed regime are analyzed with a high-speed photo-diode (electrical bandwidth 45 GHz) followed by an electrical spectrum analyzer (ESA) (electrical bandwidth 50 GHz). The laser is biased through direct probing the metal contact pads with DC needles by an external low-noise DC current source and a DC voltage supply. The laser is placed on a copper carrier temperature stabilized at 20 °C. The light-current (L-I) characteristics of the laser are presented in Fig. 2 for reverse biases of V_{SA} = 0 V (Fig. 2(a)), 1 V (Fig. 2(b)), 2 V (Fig. 2(c)) and 3 V, (Fig. 2(d)) for both propagating directions (CCW Out 1 and CW Out 4). The gain section injection current I_{SOA} is varied from 5 mA to 255 mA (increasing currents,

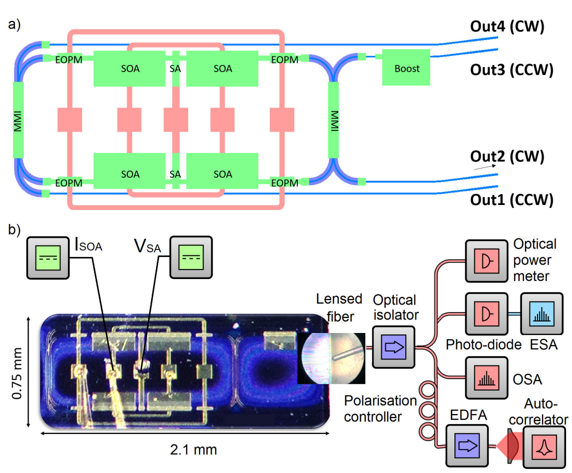

Fig. 1. (a) Blue: Passive straight and curved waveguides. Green: Active components such as semiconductor optical amplifier (SOA)-based gain sections, absorber sections (SAs), booster amplifier (Boost), and phase modulators (EOPMs), and passive components such as multimode interference (MMI) couplers. Red: Metal routing. (b) Optical microscope picture with dimensions and sketch of the experimental setup. Two DC input signals (I_{SOA} and V_{SA}) bias the active sections. Laser emission coupled by a lensed fiber is in part amplified by an erbium-doped fiber amplifier (EDFA) and studied by the measurement instruments: electrical spectrum analyzer (ESA), optical spectrum analyzer (OSA), intensity auto-correlator (right). Close-up: lensed fiber near laser facet.

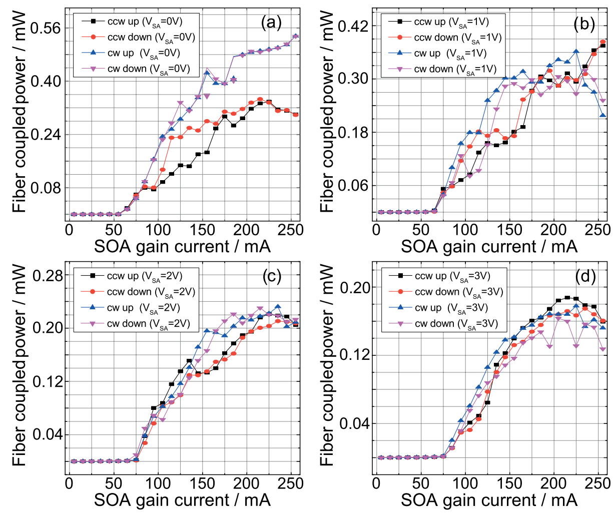

Fig. 2. Fiber-coupled average optical laser output power versus I_{SOA} at (a) V_{SA} = 0 V, (b) V_{SA} = 1 V, (c) V_{SA} = 2 V and at (d) V_{SA} = 3 V. Fiber coupling losses are ≈5 dB. Clockwise (CW, Out 4), counter-clockwise (CCW, Out 1) emission, „up“ denotes increasing and „down“ decreasing injection current. Note the different y-axis scaling.

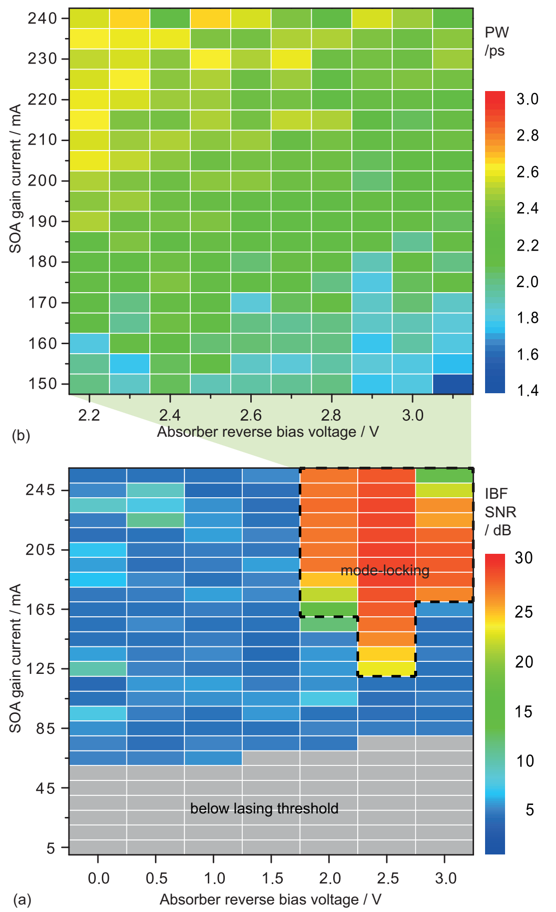

Fig. 3. Color-coded map of (a) Intermode beat frequency signal-to-noise ratio (IBF SNR) and (b) optical pulse width (PW) (within a selected biasing regime) in dependence on injected gain current and absorber reverse bias voltage.

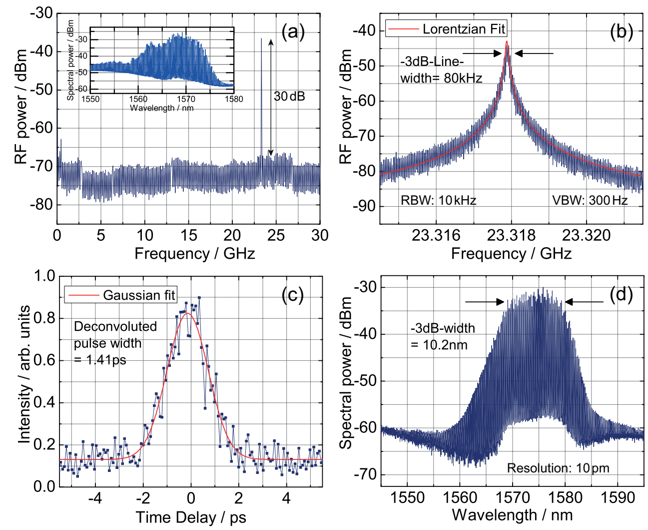

Fig. 4. (a) Full-span RF spectrum for I_{SOA} = 150 mA, V_{SA} = 3.1 V. The inset shows the optical spectrum for the same bias conditions. (b) Zoom into (a) and Lorentzian fit. (c) Auto-correlation trace at I_{SOA} = 150 mA and V_{SA} = 3.1 V. Scan range: 10 ps. (d) Optical spectrum at I_{SOA} = 215 mA, V_{SA} = 2.0 V.

„up“) and from 255 mA to 5 mA (decreasing currents, „down“) in increments of 10 mA. The results for CCW and CW indicate a threshold current of 55 mA at $V_{SA} = 0$ V, as shown in Fig. 2(a) which increases with increasing absorber reverse bias voltage up to 75 mA for $V_{SA} = 3$ V, as depicted in Fig. 2(d). The slope efficiency for CW propagation is generally higher than that for CCW propagation, yet they converge for higher bias voltages. The highest fiber-coupled power exceeds 0.5 mW for V_{SA} = 0 V for the CW direction and decreases with increasing absorber reverse bias voltage to 0.36 mW (V_{SA} = 1 V), 0.23 mW (V_{SA} = 2 V) and 0.18 mW (V_{SA} = 3 V). The CCW direction features a similar behaviour. The same fiber-coupled power is obtained at V_{SA} = 0 V and at V_{SA} = 1 V with 0.32 mW. For higher absorber reverse bias voltages 0.2 mW (V_{SA} = 2 V) and 0.18 mW (V_{SA} = 3 V) are coupled into the fiber. For both CW and CCW directions and for all investigated bias voltages, the L-I characteristics exhibit output power hysteresis behavior as depicted in Fig. 2(a)-(d), for I_{SOA} ranging from 75 mA to 250 mA. However, for the laser biasing conditions studied here, no L-I hystereses of the threshold point are observed. Next, in order to identify passive ML operation, we study first the appearance of the fundamental IBF at 23.3 GHz and its higher harmonics by RF spectra analysis and simultaneously record the RF IBF SNR which is depicted color-coded in Fig. 3(a) in dependence on injected gain current and applied absorber reverse bias voltage. I_{SOA} is varied from 5 mA to 255 mA in increments of 10 mA and V_{SA} ranging from 0 V to 3 V in increments of 0.5 V. The gray region denotes below lasing threshold operation and indicates the increase in threshold current with increasing V_{SA}. For low gain currents and low absorber reverse bias voltages (blueish colored region), low RF IBF SNRs, up to 12 dB, are identified. However, orange to red colored data points indicate IBF SNRs exceeding 15 dB. The transition between the regions is abrupt, the emission within the area indicated by a dashed line in Fig. 3(a) is regarded as passively mode-locked operation. Second, we perform detailed PW studies within the identified region of strong IBF SNR. The deconvoluted optical PWs recorded for I_{SOA} ranging from 150 mA to 240 mA and for V_{SA} ranging from 2.1 V to 3.1 V are depicted in Fig. 3(b). For all investigated biasing conditions, AC time traces indicate optical pulses that can be well fitted by well-matching Gaussian functions. Recorded PWs are well below 2.8 ps. In general, broader pulses are measured for lower reverse bias voltages, due to faster absorption recovery, and for higher injection currents, as the absorber stronger saturates and low intensity part of the pulse become less absorbed. For $I_{SOA} = 150$ mA and V_{SA} = 3.1 V, an IB LW of 80 kHz (-3 dB) at an IBF of 23.3 GHz is identified with a SNR of 30 dB, shown in Fig. 4(a). A zoom into the IBF, depicted in Fig. 4(b), depicts a pulse-to-pulse timing jitter (TJ_{ptp}) of 31.7 fs (Loretzian fit) [19, 20]. A low-frequency signature becomes apparent which is 25 dB below the IBF peak power and of spurious origin. It differs from Q-switched mode-locking as it is not apparent around the IBF. The shortest PW amounts to 1.41 ps and is obtained at I_{SOA} = 150 mA and V_{SA} = 3.1 V as shown in Fig. 4(c). Additional pulse broadening of the 1.41 ps long pulse by the EDFA (5 m internal fiber length) and 0.05-ps/nm dispersion [21] is not expected. The broadest obtained optical spectrum is centered at 1575 nm with a bandwidth of 10.2 nm (-3 dB) and 19.7 nm (-20 dB) as shown in Fig. 4(d). About 52 modes are spaced equally by 0.19 nm within the -3 dB spectral bandwidth and 102 modes within the -20 dB bandwidth. Third, we aim to study the spectral widths of the generated optical spectra in dependence on the gain currents and reverse bias

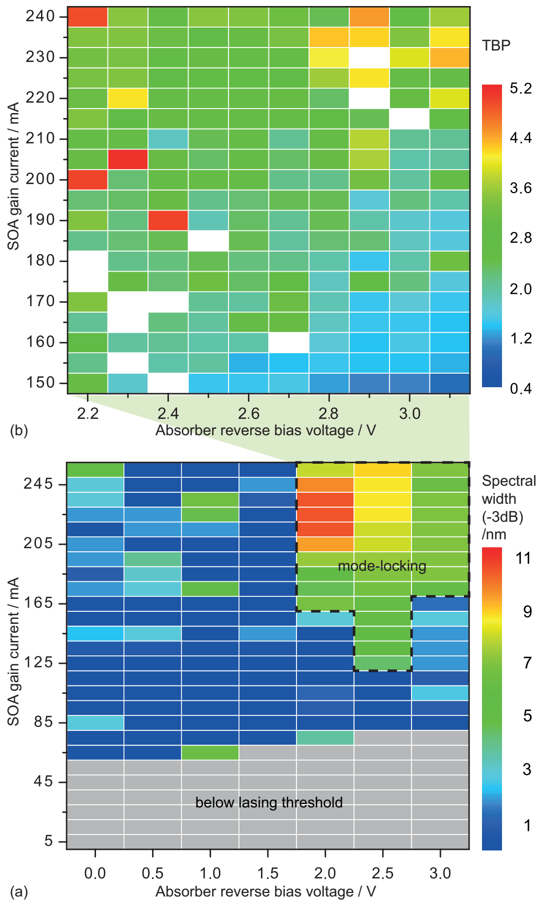

Fig. 5. Color-coded map of (a) optical spectral width (-3 dB) and (b) time-bandwidth-product (TBP) (within a selected biasing regime) in dependence on the injection current and absorber reverse bias.

voltages. For the majority of biasing conditions, the optical spectra exhibit spectrally broad, multi-modal emission for V_{SA} of 0 V, 1 V, 2 V and 3 V. A map of the acquired spectral widths (-3 dB) is depicted color-coded in Fig. 5(a) in dependence on injected I_{SOA} from 5 mA to 255 mA and on applied V_{SA} from 0 V to 3 V, corresponding to the biasing conditions selected for Fig. 3(a). Within V_{SA} >2 V and I_{SOA} >125 mA, the spectral bandwidths exceed 4.8 nm. For I_{SOA} between 205 mA and 245 mA and at V_{SA} = 2 V, bandwidths exceed 9.6 nm, indicated by orange and red color. The broadest spectrum of 10.2 nm (-3 dB) and 19.7 nm (-20 dB) is identified at V_{SA} = 2 V and I_{SOA} = 215 mA. Finally, obtained insight into the optical spectra and auto-correlation traces yield the TBP, depicted in Fig. 5(b) for the same biasing conditions as in Fig. 3(b). The TBP for I_{SOA} = 215 mA and V_{SA} = 2 V amounts to 3.06, the minimum TBP of 0.96 is measured for I_{SOA} = 150 mA and V_{SA} = 3.1 V. This operation condition coincides with the shortest measured PW of 1.41 ps. This indicates that the pulses are 2.2 times broader than expected by the Fourier transform limit. As indicated earlier, this broadening is attributed to the laser, thus future work will include to access the coherence across the modes and to evaluate the pulse chirp [16].

In conclusion, we designed and experimentally studied a photonic integrated circuit mode-locked extended cavity ring laser with two absorbers in a point symmetric geometry, manufactured in an InP-based generic foundry. Phase-locked 10.3 nm broad optical spectra been generated at an inter-mode beat frequency of 23.3 GHz. The minimum IB LW of 80 kHz corresponds to a pulse-to-pulse timing jitter of 31.7 fs. The shortest optical pulses were 1.4 ps accompanied by the lowest time-bandwidth-product value of 0.96.

FUNDING

EU Horizon 2020 Marie Skłodowska-Curie actions FiWiN5G (642355), and MULTIPLY (713694); Spanish Ministerio de Economia y Competitividad grant iTWIT (TEC2016-76997-C3-3-R); Adolf Messer Foundation (doctoral fellowship); German Research Foundation (38919332).

ACKNOWLEDGEMENTS

The authors thank E. Bente, D. Lenstra, and J. Javaloyes for fruitful discussions, W. Elsäßer for support and two anonymous reviewers for their constructive criticism.

REFERENCES

1. M. L. Davenport, S. Liu, and J. E. Bowers, Photonics Research **6**, 468 (2018).
2. V. Vujicic, A. P. Anthur, A. Saljoghei, V. Panapakkam, R. Zhou, Q. Gaimard, K. Merghem, F. Lelarge, A. Ramdane, and L. P. Barry, Optics Express **25**, 20 (2017).
3. Y.-K. Chen and M. C. Wu, IEEE Journal of Quantum Electronics **28**, 2176 (1992).
4. C. Gordón, R. Guzmán, X. Leijtens, and G. Carpintero, Photonics Research **3**, 15 (2015).
5. M.-C. Lo, R. Guzmán, and G. Carpintero, Optics Express **26**, 18386 (2018).
6. J. P. Hohimer and G. A. Vawter, Applied Physics Letters **63**, 1598 (1993).
7. E. Avrutin, J. Marsh, J. Arnold, T. Krauss, H. Pottinger, and R. D. L. Rue, IEE Proceedings - Optoelectronics **146**, 55 (1999).
8. M. Tahvili, Y. Barbarin, X. Leijtens, T. De Vries, E. Smalbrugge, J. Bolk, H. Ambrosius, M. Smit, and E. Bente, Optics Letters **36**, 2462 (2011).
9. S. Latkowski, V. Moskalenko, S. Tahvili, L. Augustin, M. Smit, K. Williams, and E. Bente, Optics Letters **40**, 77 (2015).
10. V. Moskalenko, J. Koelemeij, K. Williams, and E. Bente, Optics Letters **42**, 1428 (2017).
11. S. Yu, T. F. Krauss, and P. J. Laybourn, Optical Engineering **37**, 1164 (1998).
12. Y. Barbarin, E. A. J. M. Bente, M. J. R. Heck, Y. S. Oei, R. Nötzel, and M. K. Smit, Optics Express **14**, 9716 (2006).
13. M. Sorel, G. Giuliani, A. Scire, R. Miglierina, S. Donati, and P. J. R. Laybourn, IEEE Journal of Quantum Electronics **39**, 1187 (2003).
14. M. J. R. Heck, E. A. J. M. Bente, A. Renault, K. S. E. Eikema, W. Ubachs, R. Nötzel, Y. S. Oei, and M. K. Smit, Proc. Symposium IEEE/LEOS Benelux, Twente, Netherlands .
15. P. B. Hansen, G. Raybon, M.-D. Chien, U. Koren, B. I. Miller, M. G. Young, J.-M. Verdiell, and C. A. Burrus, IEEE Photonics Technology Letters **4**, 411 (1992).
16. V. Moskalenko, S. Latkowski, S. Tahvili, T. de Vries, M. Smit, and E. Bente, Optics Express **22**, 28865 (2014).
17. Y. Barbarin, E. Bente, M. Heck, J. Pozo, J. Rorison, Y. Oei, R. Nötzel, and M. Smit, Proceedings of the 13th European Conference on Integrated Optics (ECIO 2007), Copenhagen, Denmark **7**, 25 (2007).
18. K. Williams, E. Bente, D. Heiss, Y. Jiao, K. Ławniczuk, X. Leijtens, J. van der Tol, and M. Smit, Photonics Research **3**, B60 (2015).
19. F. Kéfélian, S. O'Donoghue, M. T. Todaro, J. G. McInerney, and G. Huyet, IEEE Photonics Technology Letters **20**, 1405 (2008).
20. L. Drzewietzki, S. Breuer, and W. Elsäßer, Optics Express **21**, 16142 (2013).
21. D. Gasper, P. Wysocki, W. Reed, and A. Vengsarkar, Proceedings of LEOS '93, San Jose, CA, USA pp. 167–168 (1993).

FULL REFERENCES

1. M. L. Davenport, S. Liu, and J. E. Bowers, "Integrated heterogeneous silicon/iii–v mode-locked lasers," Photonics Research **6**, 468–478 (2018).
2. V. Vujicic, A. P. Anthur, A. Saljoghei, V. Panapakkam, R. Zhou, Q. Gaimard, K. Merghem, F. Lelarge, A. Ramdane, and L. P. Barry, "Mitigation of relative intensity noise of quantum dash mode-locked lasers for pam4 based optical interconnects using encoding techniques," Optics Express **25**, 20–29 (2017).
3. Y.-K. Chen and M. C. Wu, "Monolithic colliding-pulse mode-locked quantum-well lasers," IEEE Journal of Quantum Electronics **28**, 2176–2185 (1992).
4. C. Gordón, R. Guzmán, X. Leijtens, and G. Carpintero, "On-chip mode-locked laser diode structure using multimode interference reflectors," Photonics Research **3**, 15–18 (2015).
5. M.-C. Lo, R. Guzmán, and G. Carpintero, "Femtosecond pulse and terahertz two-tone generation from facet-free multi-segment laser diode in inp-based generic foundry platform," Optics Express **26**, 18386–18398 (2018).
6. J. P. Hohimer and G. A. Vawter, "Passive mode locking of monolithic semiconductor ring lasers at 86 GHz," Applied Physics Letters **63**, 1598–1600 (1993).
7. E. Avrutin, J. Marsh, J. Arnold, T. Krauss, H. Pottinger, and R. D. L. Rue, "Analysis of harmonic (sub)thz passive mode-locking in monolithic compound cavity fabry-perot and ring laser diodes," IEE Proceedings - Optoelectronics **146**, 55–61(6) (1999).
8. M. Tahvili, Y. Barbarin, X. Leijtens, T. De Vries, E. Smalbrugge, J. Bolk, H. Ambrosius, M. Smit, and E. Bente, "Directional control of optical power in integrated InP/InGaAsP extended cavity mode-locked ring lasers," Optics Letters **36**, 2462–2464 (2011).
9. S. Latkowski, V. Moskalenko, S. Tahvili, L. Augustin, M. Smit, K. Williams, and E. Bente, "Monolithically integrated 2.5 ghz extended cavity mode-locked ring laser with intracavity phase modulators," Optics Letters **40**, 77–80 (2015).
10. V. Moskalenko, J. Koelemeij, K. Williams, and E. Bente, "Study of extra wide coherent optical combs generated by a QW-based integrated passively mode-locked ring laser," Optics Letters **42**, 1428–1431 (2017).
11. S. Yu, T. F. Krauss, and P. J. Laybourn, "Mode locking in large monolithic semiconductor ring lasers," Optical Engineering **37**, 1164–1169 (1998).
12. Y. Barbarin, E. A. J. M. Bente, M. J. R. Heck, Y. S. Oei, R. Nötzel, and M. K. Smit, "Characterization of a 15 GHz integrated bulk InGaAsP passively modelocked ring laser at 1.53 µm," Optics Express **14**, 9716–9727 (2006).
13. M. Sorel, G. Giuliani, A. Scire, R. Miglierina, S. Donati, and P. J. R. Laybourn, "Operating regimes of GaAs-AlGaAs semiconductor ring lasers: experiment and model," IEEE Journal of Quantum Electronics **39**, 1187–1195 (2003).
14. M. J. R. Heck, E. A. J. M. Bente, A. Renault, K. S. E. Eikema, W. Ubachs, R. Nötzel, Y. S. Oei, and M. K. Smit, "5-GHz passively mode-locked quantum dot ring laser diode at 1.5 μm," Proc. Symposium IEEE/LEOS Benelux, Twente, Netherlands .
15. P. B. Hansen, G. Raybon, M.-D. Chien, U. Koren, B. I. Miller, M. G. Young, J.-M. Verdiell, and C. A. Burrus, "A 1.54 μm monolithic semiconductor ring laser: CW and mode-locked operation," IEEE Photonics Technology Letters **4**, 411–413 (1992).
16. V. Moskalenko, S. Latkowski, S. Tahvili, T. de Vries, M. Smit, and E. Bente, "Record bandwidth and sub-picosecond pulses from a monolithically integrated mode-locked quantum well ring laser," Optics Express **22**, 28865–28874 (2014).
17. Y. Barbarin, E. Bente, M. Heck, J. Pozo, J. Rorison, Y. Oei, R. Nötzel, and M. Smit, "18 GHz fabry-pérot integrated extended cavity passively modelocked lasers," Proceedings of the 13th European Conference on Integrated Optics (ECIO 2007), Copenhagen, Denmark **7**, 25–27 (2007).
18. K. Williams, E. Bente, D. Heiss, Y. Jiao, K. Ławniczuk, X. Leijtens, J. van der Tol, and M. Smit, "InP photonic circuits using generic integration," Photonics Research **3**, B60–B68 (2015).
19. F. Kéfélian, S. O'Donoghue, M. T. Todaro, J. G. McInerney, and G. Huyet, "RF linewidth in monolithic passively mode-locked semiconductor laser," IEEE Photonics Technology Letters **20**, 1405–1407 (2008).
20. L. Drzewietzki, S. Breuer, and W. Elsäßer, "Timing jitter reduction of passively mode-locked semiconductor lasers by self- and external-injection: Numerical description and experiments," Optics Express **21**, 16142–16161 (2013).
21. D. Gasper, P. Wysocki, W. Reed, and A. Vengsarkar, "Evaluation of chromatic dispersion in erbium-doped fibers," Proceedings of LEOS '93, San Jose, CA, USA pp. 167–168 (1993).